ISSN 2176-5480

22nd International Congress of Mechanical Engineering (COBEM 2013)
November 3-7, 2013, Ribeirão Preto, SP, Brazil

GAS-SURFACE INTERACTION IMPACT ON AERODYNAMIC HEATING OF A REENTRY BRAZILIAN CAPSULE

Wilson F. N. Santos
Combustion and Propulsion Laboratory (LCP)
National Institute for Space Research (INPE)
Cachoeira Paulista-SP, 12630-000 BRAZIL
wilson@lcp.inpe.br

Abstract. *This work presents a computational analysis of the gas-surface interaction impact on the prediction of the main aerodynamic surface loads of a space reentry capsule. In the present work different surface accommodation coefficients have been simulated by using the Direct Simulation Monte Carlo (DSMC) method in conjunction with the Cercignani-Lampis-Lord gas surface interaction model. The DSMC calculations examine differences in predictions of aerodynamic forces and heat transfer between full and partial surface accommodations for a hypersonic flow past to the Brazilian prototype reentry capsule SARA (acronym for SAtélite de Reentrada Atmosférica). Seven combinations of normal and tangential accommodation coefficients associated to five different altitudes were used in the simulation. For the flow conditions considered, the analysis showed that stagnation point heating are sensitive to changes on either normal or tangential accommodation coefficients. Results substantiate that it becomes imperative to take surface accommodation into account in order to make accurate predictions of the aerodynamic forces acting on the capsule surface, and of the heat transfer rates to the surface of the capsule at hypersonic flow.*

Keywords: *DSMC, Hypersonic flow, Rarefied flow, Reentry capsule, SARA.*

1. INTRODUCTION

The correct prediction of the aerothermodynamic aspects of reentry vehicles along their entire trajectory is often an important step in their design phase. In the Earth atmosphere reentry, vehicles undergo not only different velocity regimes – hypersonic, supersonic and subsonic – but also different flow regimes – free molecular flow, transition and continuum – and flight conditions that may difficult their aerodynamic design. In the molecular flow or in the transition flow regime, hypersonic vehicles may encounter non-equilibrium conditions which can have a significant influence on the aerodynamic performance. An understanding of these flow phenomena can be gained by flight testing and wind-tunnel testing. Nevertheless, both testings are expensive and danger. These factors are mitigated by computer simulations. Certainly, computer simulations can not eliminate physical experimentation. However, they can greatly reduce the amount of such experimentation. In addition, numerical techniques, which fail to incorporate non-equilibrium conditions, miss out on an essential part of the flow physics surrounding the reentry vehicle.

Many numerical studies and a few experimental investigations (Gilmore and Crowther, 1995; Gupta *et al.*, 1996; Wood *et al.*, 1996; Wilmoth *et al.*, 1997; Ivanov *et al.*, 1998; Carlson, 1999; Gnoffo, 1999; Vashchenkov and Ivanov, 2002; Longo, 2003; Weiland *et al.*, 2004; Savino *et al.*, 2005; Moss, 2006) have been dedicated to the aerothermodynamics of vehicles reentering the Earth atmosphere. Nevertheless, for the particular case of SARA capsule, only a few studies are available in the current literature (Toro *et al.*, 2001; Sharipov, 2003; Toro *et al.*, 2004; Pimentel *et al.*, 2005; Tchuen *et al.*, 2005; Kozak and Sharipov, 2012; Santos, 2012). For the purpose of this introduction, it will be sufficient to describe only a few of these studies.

Pimentel *et al.* (2005) have performed inviscid hypersonic flow simulations over the SARA capsule by employing the planar two-dimensional (2-D) and the axisymmetric Euler equations. Results were presented for an altitude of 80 km, Mach numbers of 15 and 18, and angle of attack of 0 and 10 degrees. They also considered air as the working fluid composed of five species (N_2, O_2, O, N, and NO) with their reactions of dissociation and recombination. Pressure and temperature contour maps were presented for 2-D and axisymmetric flow.

Tchuen *et al.* (2005) have investigated the flowfield structure over the SARA capsule by using axisymmetric Navier-Stokes equations. The analysis considered hypersonic flow at zero angle of attack in chemical and thermal non-equilibrium. It was assumed air as the working fluid composed of seven species (N_2, O_2, O, N, NO, NO^+, and e^-) associated with their reactions of dissociation and recombination. Results for pressure, skin friction, and heat transfer coefficients were presented for different combinations of Mach numbers of 10, 20 and 25 with altitudes of 75 and 80 km.

Finally, Santos (2012) has investigated the flowfield structure of a hypersonic flow over the SARA capsule in the reentry trajectory, from 100 km to 80 km, by employing the DSMC method. This range basically covered the transition flow regime, *i.e.*, between the free collision flow and the continuum flow regime. The primary goal was to assess the sensitivity of the primary properties, velocity, density, pressure, and temperature due to changes on the altitude representative of a typically reentry trajectory of the SARA capsule. The investigation considered two species (N_2 and O_2) as the working

ISSN 2176-5480

fluid, and rotation and vibration internal modes of energy.

The previous work (Santos, 2012) on hypersonic flow past SARA capsule has concentrated primarily on the analysis of the flowfield structure by considering the diffuse reflection model as being the gas-surface interaction. The diffuse model assumes that the molecules are reflected equally in all directions, quite independently of their incident speed and direction. Nevertheless, as a space flight vehicle is exposed to a rarefied environment over a considerable time, a departure from the fully diffuse model is observed, resulting from colliding molecules that clean the surface of the vehicle, which becomes gradually decontaminated. Molecules reflected from clean surfaces show lobular distribution in direction. The flux distribution of scattered molecules emitted from clean surfaces frequently has a lobular shape that is centered about an angle, which tends to approach the specular angle for very high energies and/or low angle of attack (Bird, 1994).

In this scenario, the present account extends the previous analysis (Santos, 2012) by examining the gas-surface interaction impact on aerodynamic surface quantities of the SARA capsule for the same reentry conditions. In this fashion, the primary goal of this study is to assess the sensitivity of the heat transfer, pressure, skin friction, and drag coefficients due to variations in the surface accommodation coefficients by employing the Cercignani-Lampis-Lord (CLL) model (Lord, 1991). The CLL model, which incorporates independent accommodation coefficients for the normal and tangential velocity components, is implemented into the DSMC code, and simulations are performed by assuming the axisymmetric hypersonic flow over the SARA capsule.

2. GAS-SURFACE INTERACTION MODEL

The successful application of the DSMC method requires the development of an accurate gas-surface interaction model besides a gas-gas molecular collision model. As the majority of the practical engineering problems involves gas-surface interaction phenomena, a suitable boundary condition is required in order to obtain reliable results from numerical simulation of rarefied gas flows. Three models of gas-surface interactions may be employed in the DSMC method as practical models for purpose of engineering surfaces: (1) specular reflection, (2) diffuse reflection, and (3) some combination of these. In a specular reflection, molecules are reflected like a perfectly elastic sphere with reversal of the normal component of velocity and no change in the parallel component of velocities and energy. In a diffuse reflection, the molecules are reflected equally in all directions usually with a complete thermal accommodation. The final velocity of the molecules is randomly assigned according to a half-range Maxwellian distribution determined by the wall temperature. The combination of diffuse reflection with specular reflection, known as Maxwell model (Maxwell, 1879), introduces a single parameter f to indicate the fraction of those molecules reflected diffusely in a completely accommodated fashion according to a Maxwellian distribution corresponding to the wall temperature, and the remaining fraction $(1-f)$, being assumed to reflect specularly. Usually, the parameter f in the Maxwell model is identified by the tangential accommodation coefficient σ_t.

The popularity of the Maxwell model (Maxwell, 1879) is explained apparently by its simplicity and by the fact that it satisfies reciprocity, i.e., the principle of detailed balance. A phenomenological model that also satisfies the reciprocity conditions and has demonstrated improvement over the Maxwell model has been proposed by Cercignani and Lampis (1971), known as CL model. This model is based on the definition of two parameters α_n and σ_t that represent the accommodation coefficient for the kinetic energy associated with the normal component of velocity, and the parallel momentum accommodation, respectively. They are given by the following equations,

$$\alpha_n = \frac{e_i - e_r}{e_i - e_w} \tag{1}$$

$$\sigma_t = \frac{\tau_i - \tau_r}{\tau_i} \tag{2}$$

where e and τ refer to the average kinetic energy for the normal component of velocity, and momentum flux acting tangential to the surface, respectively; subscripts i and r stand for the incident and reflected components, and w refers to the component that would be produced by a diffuse reflection at the surface temperature.

The CL model provides a continuous spectrum of behavior from specular reflection at one end to diffuse reflection with complete energy accommodation at the other, and produces physically realistic distributions of direction and energy re-emitted molecules.

The probability distribution function for the component of velocity normal to the surface is given by,

$$P_n(v_n'|v_n) = \frac{2v_n'}{\alpha_n} I_0\left(2\sqrt{1-\alpha_n}\frac{v_n v_n'}{\alpha_n}\right) \exp\left[-\frac{v_n'^2 + (1-\alpha_n)v_n^2}{\alpha_n}\right] \tag{3}$$

where I_0 is the modified Bessel function, v_n' and v_n are the incident and reflect velocity components normalized by the most probable molecular speed at the surface temperature, and defined by $\sqrt{2kT_w/m}$.

ISSN 2176-5480

The probability distribution function for the component of velocity parallel to the surface is given by,

$$P_t(\mathbf{v}'_t|\mathbf{v}_t) = \frac{1}{\sqrt{\pi\sigma_t(2-\sigma_t)}} \exp\{-\frac{v'_t - (1-\sigma_t)v_t]^2}{\pi\sigma_t(2-\sigma_t)}\} \tag{4}$$

where $\mathbf{v}'_t$ and $\mathbf{v}_t$ are the incident and reflect tangential velocity vector also normalized by the most probable molecular speed at the surface temperature.

Lord (1991) has implemented the CL model into the DSMC method, and presented a simple method for generating random sample velocities from Eqs. (3) and (4). The DSMC method with Lord's implementation is referred as the Cercignani-Lampis-Lord (CLL) model. For comparison purpose, Fig. 1 displays a schematic drawing representing the Maxwell reflection model and the CLL reflection model.

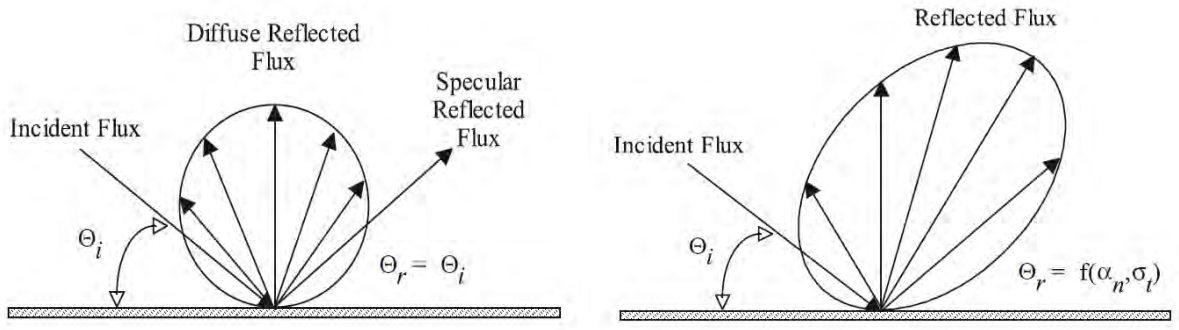

(a) **Maxwell Model** (b) **CLL Model**

Figure 1. Drawing illustrating the Maxwell reflection model and the CLL reflection model.

It should be emphasized the CLL model was derived by assuming that there is no coupling between the normal and tangential momentum components. The two adjustable parameters appearing in the CLL model are the normal component of translational energy α_n and the tangential component of momentum σ_t. However, in the implementation of the CLL model in the DSMC method, Bird (1994) has shown that it is equivalent to specify the normal α_n and tangential α_t components of translational energy, since $\alpha_t = \sigma_t(2-\sigma_t)$, and thus that $\sigma_t < \alpha_t$, by assuming that σ_t lies between 0 and 1. In the present account, α_n and σ_t are used as being the two adjustable parameters.

Before proceeding with the analysis, it is important to mention that many studies have been made using both the CL and the CLL models to analyze the behavior of molecules reflected from surface. Of particular interest are the application of the CL model described in Cercignani (1972) and those on CLL model discussed by Woronowicz and Rault (1994) and Hedahl and Wilmoth (1995).

3. COMPUTATIONAL TOOL

In the analysis of aerothermodynamic characteristics of aerospace vehicles, along their descending flight trajectory through the Earth atmosphere, different computational methods are required. At high altitudes, the aerothermodynamic predictions are related to the free molecular or to transition flow regime. In the transition flow regime, the Direct Simulation Monte Carlo (DSMC) method is usually employed. At low altitudes, the aerothermodynamic predictions are related to the continuum flow regime. In this regime, computational methods such as Computational Fluid Dynamics (CFD) are employed. In the present account, the vehicle is subjected to the conditions characterized by the transition flow regime. In this fashion, DSMC method is the suitable computational tool in order to investigate the aerothermodynamic characteristics.

The DSMC method, pioneered by Bird (1994), simulates real gas flows with various physical processes by means of a huge number of modeling particles, each of which is a typical representative of a great number of real gas molecules. The reason for that is because it is unfeasible to simulate the real number of particles present in real gases. The state of the modeling particles, position, velocity and internal energy, is stored and modified with time as the particles move, collide, and undergo boundary interactions in the simulated physical space. The simulation is always calculated as unsteady flow. However, the boundary conditions can be applied such that steady flow solution is obtained as the outcome of the large time state of the unsteady flow.

The DSMC method conditionally divides the continuous process of particles movement and collisions into two consecutive stages at each small time step. In the first stage, moving process, all modeling particles are propagated for a time

ISSN 2176-5480

step without collisions. In the second stage, collision process, some randomly chosen pairs of particles in the same cell are allowed to collide and change their velocities without changing their positions. The physical assumption behind this approximation is that the gas is considered as a dilute one. It means that the mean molecular diameter is much smaller than the mean molecular spacing of the gas. In addition, molecular caos is the other assumption behind the method. It means that position and velocities of randomly picked particles are uncorrelated.

Collisions in the present DSMC code are modeled by using the variable hard sphere (VHS) molecular model (Bird, 1981) and the no time counter (NTC) collision sampling technique (Bird, 1989). Repartition energy among internal and translational modes is controlled by the Larsen-Borgnakke statistical model (Borgnakke and Larsen, 1975). Simulations are performed using a non-reacting gas model for a constant freestream gas composition consisting of 76.3% of N_2 and 23.7% of O_2. Energy exchanges between the translational and internal modes, rotational and vibrational, are considered. The probability of an inelastic collision determines the rate at which energy is transferred between the translational and internal modes after an inelastic collision. For a given collision, the probability is defined by the inverse of the number of relaxation, which corresponds to the number of collisions needed, on average, for a molecule to undergo relaxation. In the present account,relaxation collision numbers of 5 and 50 were used for the calculations of rotation and vibration, respectively.

4. GEOMETRY DEFINITION

In the present account, the SARA capsule geometry follows that one defined in the previous study (Santos, 2012). The capsule is an axisymmetric design consisting of a spherical nose with a 11.4-degree half-angle conical afterbody. The nose radius R is 0.2678 m, the afterbody base has a radius R_B of 0.5035 m, and the total length L is 1.410 m. Figure 2(a) illustrates schematically the capsule shape and the main important physical and geometric parameters related to the hypersonic flow on the capsule. The main physical parameters are defined as follows: M_∞ is the freestream Mach number, Kn_∞ stands for the Knudsen number, T_w is the wall temperature, and finally, α_n and σ_t are the accommodation coefficients.

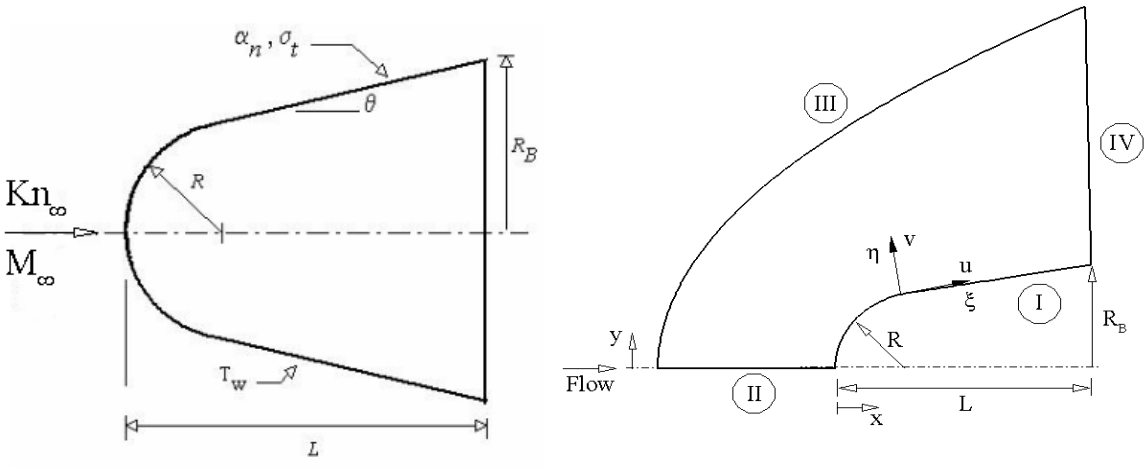

(a) (b)

Figure 2. Drawing illustrating (a) a schematic view of the capsule and (b) the computational domain.

5. FREESTREAM AND FLOW CONDITIONS

Freestream flow conditions are those given in the previous investigation (Santos, 2012) and summarized in Tab. 1, and the gas properties (Bird, 1994) are tabulated in Tab. 2. Based on this set of tables, T_∞, p_∞, ρ_∞, n_∞, λ_∞, and V_∞ represent, respectively, temperature, pressure, density, number density, molecular mean free path, and velocity. In addition, χ, m, d and ω stand respectively for mass fraction, molecular mass, molecular diameter and viscosity index.

The freestream velocity V_∞ of 7862, 7866, 7864, 7864, and 7820 m/s, for altitude of 100, 95, 90, 85, and 80 km is based on the velocity-altitude map for the SARA capsule (Santos, 2012). In addition, these values correspond to a freestream Mach number M_∞ of 27.1, 28.1, 29.2, 29.2, and 29.0, respectively.

ISSN 2176-5480

Table 1. Freestream flow conditions (Santos, 2012).

Altitude (km)	T_∞(K)	p_∞(N/m^2)	ρ_∞(kg/m^3)	n_∞(m^{-3})	λ_∞(m)	V_∞(m/s)
80	180.7	1.03659	1.999×10^{-5}	4.1562×10^{21}	3.085×10^{-3}	7820
85	180.7	0.41249	7.956×10^{-6}	1.6539×10^{20}	7.751×10^{-3}	7864
90	180.7	0.16438	3.171×10^{-6}	6.5908×10^{19}	1.945×10^{-2}	7864
95	195.5	0.06801	1.212×10^{-6}	2.5197×10^{19}	5.088×10^{-2}	7866
100	210.0	0.03007	4.989×10^{-7}	1.0372×10^{19}	1.236×10^{-1}	7862

Table 2. Gas properties (Bird, 1994).

	χ	m (kg)	d (m)	ω
O_2	0.237	5.312×10^{-26}	4.01×10^{-10}	0.77
N_2	0.763	4.650×10^{-26}	4.11×10^{-10}	0.74

For the altitudes investigated, 100, 95, 90, 85, and 80 km, the overall Knudsen number, defined as the ratio of the freestream molecular mean free path λ_∞ to the nose radius R, corresponds to Kn_R of 0.4615, 0.1899, 0.0726, 0.0289, and 0.0115, respectively. The Reynolds number Re_R correspond to 92, 224, 609, 3442 and 15249 for altitudes of 100, 95, 90, 85 and 80 km, respectively, based on conditions in the undisturbed stream with the nose radius R as the characteristic length. Finally, the capsule surface was kept at a constant wall temperature T_w of 800 K for all cases investigated.

In order to simulate the incomplete surface accommodation, the CLL model implemented into the DSMC code considered only the normal and tangential accommodation coefficients. The internal energy accommodation was kept equal to one for all calculations presented in this work. Hence, α_n and σ_t are used as being the two adjustable parameters. The DSMC calculations were performed independently for four distinct numerical values for α_n and σ_t: 0.25, 0.50, 0.75, and 1. Therefore, when α_n is equal to 0.25, 0.50 or 0.75, σ_t is set equal to 1, and vice-versa. It is important to mention that $\alpha_n = 1 = \sigma_t$ represents the diffusion reflection case.

6. COMPUTATIONAL FLOW DOMAIN AND GRID

A schematic view of the computational domain is demonstrated in Fig. 2(b). Advantage of the flow symmetry is taken into account, and molecular simulation is applied to one-half of a full configuration. The computational domain used for the calculation is made large enough so that the capsule disturbances do not reach the upstream and side boundaries, where freestream conditions are specified. In this fashion, the computational domain changed according to the rarefaction degree of the flow on the capsule.

The computational domain around the capsule is divided into an arbitrary number of regions, which are subdivided into computational cells. The cell provides a convenient reference for the sampling of the macroscopic gas properties. In addition, the cells are further subdivided into subcells. The subcell provides a reference for the collision process. The collision partners are selected from the same subcell in order to establish the collision rate. In the present investigation, it was defined two subcells/cell in each coordinate direction. As a result, the physical space network is used to facilitate the choice of molecules for collisions as well as for the sampling of the macroscopic flow properties, such as temperature, pressure, density, etc.

According to Fig. 2(b), side I is defined by the capsule surface. Reflection with incomplete surface accommodation is the condition applied to this side. Side II is a plane of symmetry, where all flow gradients normal to the plane are zero. At the molecular level, this plane is equivalent to a specular reflecting boundary. Side III is the freestream side through which simulated molecules enter and exit. Finally, the flow at the downstream outflow boundary, side IV, is predominantly supersonic and vacuum condition was assumed at this boundary (Bird, 1994). As a result, simulated molecules can only exit at this boundary. It is important to remark that, close to the wall, molecules may not be moving at supersonic speed. Consequently, in this subsonic region close to the wall, there is an interaction between the flow and the downstream boundary. Nevertheless, the extent of the upstream effect of this boundary condition can be determined by changing the length of the cone surface. In doing so, it was found that the upstream disturbance is approximately of $2\lambda_\infty$ for the altitudes investigated.

The numerical accuracy in DSMC method depends on the cell size chosen, on the time step as well as on the number of particles per computational cell. In the DSMC algorithm, the linear dimensions of the cells should be small in comparison with the length scale of the macroscopic flow gradients normal to streamwise directions. Therefore, the cell dimensions

ISSN 2176-5480

should be the order of or smaller than the local mean free path (Alexander *et al.*, 1998, 2000). Furthermore, the time step should be chosen to be sufficiently small in comparison with the local mean collision time (Garcia and Wagner, 2000; Hadjiconstantinou, 2000). In general, the total simulation time, discretized into time steps, is based on the physical time of the real flow. Finally, the number of simulated particles has to be large enough to make statistical correlations between particles insignificant.

These effects were investigated in order to determine the time steps, the number of cells, and the number of particles required to achieve grid independent solutions. Grid independence was tested by running the calculations with three different structured meshes – coarse, standard and fine – in each coordinate direction. The effect of altering the cell size in the ξ-direction was investigated for a coarse and fine grids with, respectively, 50% less and 100% more cells with respect to the standard grid only in the ξ-direction. In analogous fashion, an examination was made in the η-direction with a coarse and fine grids with, respectively, 50% less and 100% more cells with respect to the standard grid only in the η-direction. In addition, each grid was made up of non-uniform cell spacing in both directions. Moreover, point clustering was used close to capsule surface. Heat transfer, pressure and skin friction coefficients were selected in order to elucidate the requirements posed for the grid sensitivity study. Distributions of these surface properties for the three grids were basically the same, an indication that the standard grid was rather insensitive to the range of cell spacing considered. A discussion of these effects on the aerodynamic surface properties is described in details by Santos (2012).

As part of the validation process, the axisymmetric version of this DSMC code was applied to a flat-ended circular cylinder in a rarefied hypersonic flow. Results for velocity, translational temperature, and rotational temperature distributions along the stagnation streamline were presented and compared with those obtained from another established DSMC code based in a code-to-code comparison. Again, this comparison is described in details by Santos (2012). Therefore, it will not be shown in this work.

7. COMPUTATIONAL RESULTS AND DISCUSSION

Incomplete surface accommodation effects on the aerodynamic surface quantities acting on the SARA capsule are demonstrated in this section by comparing simulated results for altitudes of 100, 95, 90, 85 and 80 km, which correspond to freestream Knudsen numbers of 0.4615, 0.1899, 0.0726, 0.0289, and 0.0115, respectively. Aerodynamic surface quantities of particular interest in the transition flow regime are number flux, heat flux, wall pressure, shear stress, and drag.

7.1 Number Flux

The number flux N is calculated by sampling the molecules impinging on the surface by unit time and unit area. The distribution of the number flux along the capsule surface is illustrated in Figs. 3(a-c) for altitudes of 100, 90 and 80 km, respectively. In this group of plots, dimensionless arc length is the arc length s normalized by the nose radius R, and N_f represents the number flux N normalized by $n_\infty V_\infty$, where n_∞ is the freestream number density and V_∞ is the freestream velocity. In addition, filled symbols correspond to the accommodation coefficient σ_t and empty symbols the coefficient α_n. As a base of comparison, the dimensionless number flux for the diffuse reflection case is also presented in this set of plots. It is important to mention that results for 85 km and 95 km cases are intermediate to those for 100 km and 80 km and, therefore, they will no be shown.

According to this set of plots, it is seen that the number flux N_f to the surface depends not only on the altitude (or

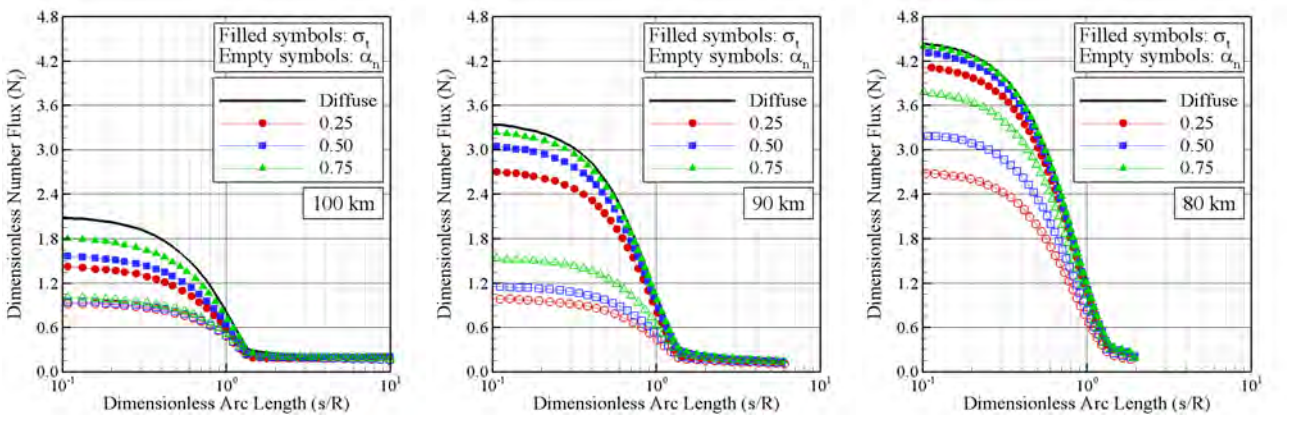

Figure 3. Dimensionless number flux (N_f) distribution along the capsule surface as a function of the surface accommodation coefficients for altitudes of (a) 100 km, (b) 90 km, and (c) 80 km.

ISSN 2176-5480

Knudsen number) but also on the gas-surface interaction. In general, the curves show two distinct regions: one inner region, along the spherical nose, and an outer region, along the cone surface. In the inner region, at the vicinity of the stagnation point, the number flux is basically constant and presents its maximum value. In addition, in this region, the number flux increases significantly with decreasing the altitude, i.e., by decreasing the Knudsen number. This increase in the dimensionless number flux N_f with decreasing the altitude may be related to the collisions of two groups of molecules: the molecules reflecting from the capsule surface and the molecules oncoming from freestream. The molecules that are reflected from the capsule surface, which have low kinetic energy, interact with the oncoming freestream molecules, which have high kinetic energy. Thus, the surface-reflected molecules collide again with the capsule surface, which produce an increase in the dimensionless number flux in the stagnation region. As expected, this behavior is less pronounced by a reduction on the normal α_n or on the tangential σ_t accommodation coefficients, since the molecules are reflected from the surface with different energies. Consequently, the net buildup of particle density near the capsule surface is reduced.

7.2 Heat Transfer Coefficient

The heat transfer coefficient C_h is defined as follows,

$$C_h = \frac{q_w}{\frac{1}{2}\rho_\infty V_\infty^3} \tag{5}$$

where the heat flux q_w to the body surface is calculated by the net energy flux of the molecules impinging on the surface. A flux is regarded as positive if it is directed toward the body surface. The net heat flux q_w is related to the sum of the translational, rotational and vibrational energies of both incident and reflected molecules as defined by,

$$q_w = q_i - q_r = \frac{F_N}{A\Delta t}\{\sum_{j=1}^{N}[\frac{1}{2}m_j c_j^2 + e_{Rj} + e_{Vj}]_i - \sum_{j=1}^{N}[\frac{1}{2}m_j c_j^2 + e_{Rj} + e_{Vj}]_r\} \tag{6}$$

where F_N is the number of real molecules represented by a single simulated molecule, Δt is the time step, A the area, N is the number of molecules colliding with the surface by unit time and unit area, m is the mass of the molecules, c is the velocity of the molecules, e_R and e_V stand for rotational and vibrational energies, respectively. Subscripts i and r refer to incident and reflect molecules.

The dependence of the heat transfer coefficient C_h on the gas-surface interaction is demonstrated in Figs. 4(a-c) for altitude of 100, 90 and 80 km, respectively. Based on this set of diagrams, it is clearly noticed that the heat transfer coefficient C_h is sensitive not only to the gas-surface interaction but also to the altitude, $i.e.$, to the Knudsen number Kn_R. In general, the heat transfer coefficient C_h presents the maximum value at the stagnation point. After that, a short distance away from the stagnation point, it drops off up to the sphere/cone junction. It is also seen that as the altitude decreases, $i.e.$, the Knudsen number decreases, the heat transfer coefficient C_h decreases for the conditions investigated in this work. As the altitude decreases, the freestream density significantly increases (Santos, 2012), and the denominator in Eq. (5) increases. Consequently, a decrease in the heat transfer coefficient C_h is observed.

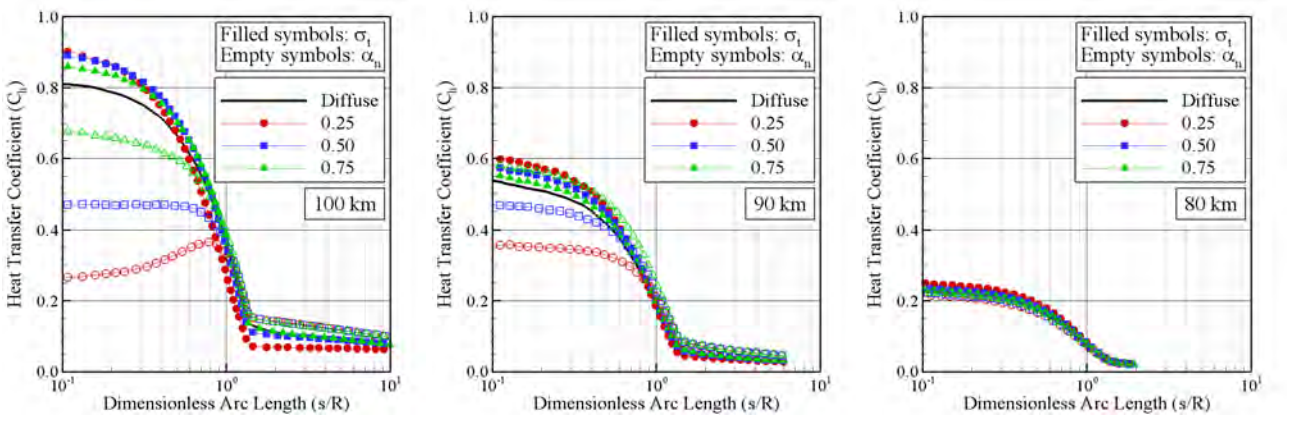

Figure 4. Heat transfer coefficient (C_h) distribution along the capsule surface as a function of the surface accommodation coefficients for altitudes of (a) 100 km, (b) 90 km, and (c) 80 km.

ISSN 2176-5480

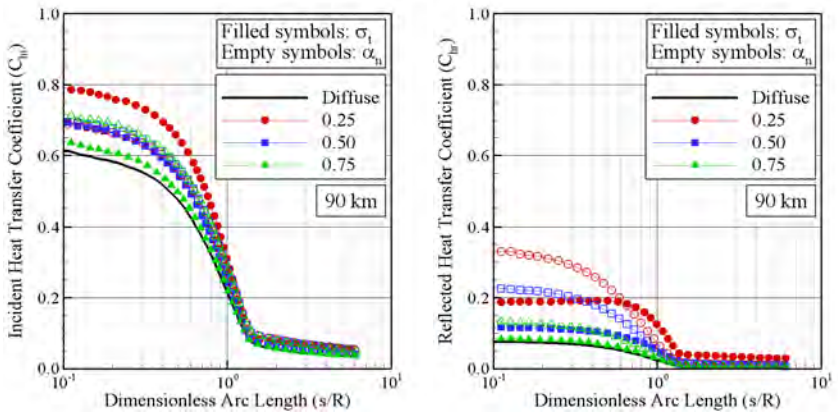

Figure 5. (a) Incident heat transfer coefficient C_{hi} and (b) reflected heat transfer coefficient C_{hr} along the capsule surface as a function of the surface accommodation coefficients for altitude of 90 km.

Still referring to Figs. 4(a-c), it is noticed the heat transfer coefficient decreases with decreasing the normal accommodation coefficient α_n. In contrast, the heat transfer coefficient increases with decreasing the tangential accommodation coefficient σ_t. An understanding of this opposite behavior can be gained by considering independently the contribution of the incident and reflected heat fluxes that appear in Eq. (6). In this scenario, Figs. 5(a,b) depict, respectively, the incident and reflected components of the heat flux for the altitude of 90 km in terms of the incident C_{hi} and reflected C_{hr} heat transfer coefficients.

According to Figs. 5(a,b), it is observed that a reduction in the normal accommodation coefficient α_n as well as in the tangential accommodation coefficient σ_t contributes to increases the incident heat flux along the spherical nose surface as compared to that for the diffuse reflection case. In addition, a reduction in both coefficients, α_n and σ_t, also contributes to increase the reflected heat transfer coefficient. Nevertheless, the reflect heat transfer coefficient increases much more for changes in the normal accommodation than for changes in the tangential accommodation coefficient. As a result, the net heat flux is lower than that for the diffuse reflection case with decreasing the normal accommodation coefficient α_n, and it is larger than that for the diffuse reflection case with decreasing the tangential accommodation coefficient σ_t.

7.3 Pressure Coefficient

The pressure coefficient C_p is defined as follows,

$$C_p = \frac{p_w - p_\infty}{\frac{1}{2}\rho_\infty V_\infty^2} = \frac{p_w/p_\infty - 1}{\frac{1}{2}\gamma_\infty M_\infty^2} \tag{7}$$

where γ_∞ is the freestream specific heat ratio, and the pressure p_w on the body surface is calculated by the sum of the normal momentum fluxes of both incident and reflected molecules at each time step as follows,

$$p_w = p_i - p_r = \frac{F_N}{A\Delta t}\sum_{j=1}^{N}\{[(mv)_j]_i - [(mv)_j]_r\} \tag{8}$$

where v is the velocity component of the molecule j in the surface normal direction.

The impact of rarefaction on the pressure coefficient C_p along the capsule surface as a function of the dimensionless arc length s/R is depicted in Figs. 6(a-c) for 100, 90 and 80 km of altitude, respectively.

On examining Figs. 6(a-c), it is observed that the pressure coefficient C_p acting on the SARA capsule surface follows the same trend as that presented by the number flux and by the heat transfer coefficient in the sense that C_p is maximum in the stagnation region. After that, C_p drastically decreases up to the sphere/cone junction. Along the conical afterbody surface, the pressure coefficient C_p is basically constant, with values one order of magnitude lower than those attained in the stagnation point region. In addition, this set of plots demonstrates that the pressure coefficient C_p increases significantly at the vicinity of the stagnation point for high altitude with reducing the normal accommodation coefficient α_n. In contrast, no appreciable changes are observed on C_p for the low altitude investigated. Consequently, the pressure coefficient is a sensitive function of the altitude when the normal accommodation coefficient α_n is reduced from 1 to 0.25. One possible reason for this higher surface pressure might be that molecules that are reflected upstream in the stagnation

ISSN 2176-5480

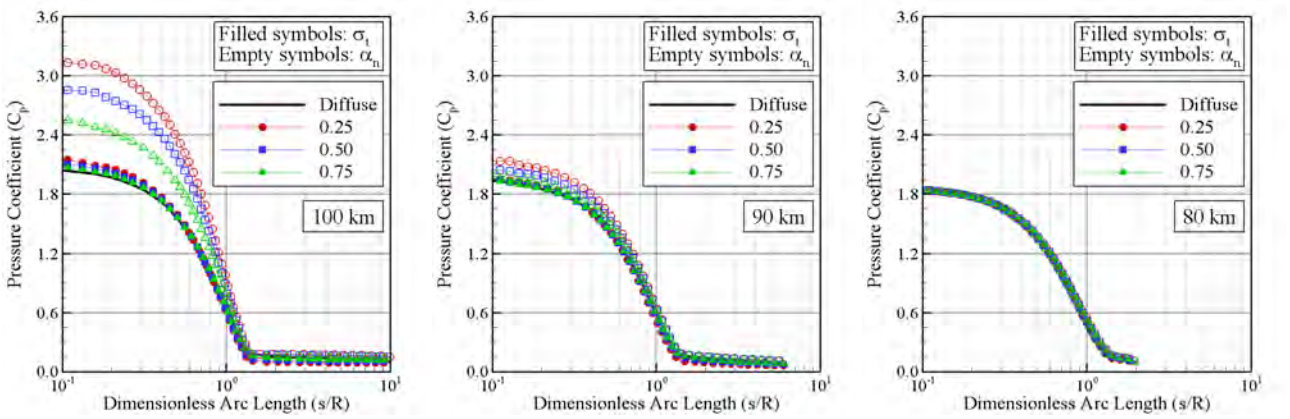

Figure 6. Pressure coefficient (C_p) distribution along the capsule surface as a function of the surface accommodation coefficients for altitudes of (a) 100 km, (b) 90 km, and (c) 80 km.

region have a high kinetic energy with the partial accommodation model and, thus, when they recollide with the surface, they will impart a greater normal moment transfer. Moreover, it may also be recognized from Figs. 6(a-c) that the pressure coefficient C_p is basically insensitive to changes in the tangential accommodation coefficient σ_t.

7.4 Skin Friction Coefficient

The skin friction coefficient C_f is defined as follows,

$$C_f = \frac{\tau_w}{\frac{1}{2}\rho_\infty V_\infty^2} = \frac{\tau_w / p_\infty}{\frac{1}{2}\gamma_\infty M_\infty^2} \tag{9}$$

where the shear stress τ_w on the body surface is calculated by the sum of the tangential momentum fluxes of both incident and reflected molecules impinging on the surface at each time step by the following expression,

$$\tau_w = \tau_i - \tau_r = \frac{F_N}{A\Delta t}\sum_{j=1}^{N}\{[(mu)_j]_i - [(mu)_j]_r\} \tag{10}$$

where u is the velocity component of the molecule j in the surface tangential direction.

The rarefaction effect on the skin friction coefficient C_f along the SARA capsule surface is demonstrated in Figs. 7(a-c) for altitudes of 100, 90 and 80 km, respectively. Along the capsule surface, C_f starts from zero at the stagnation

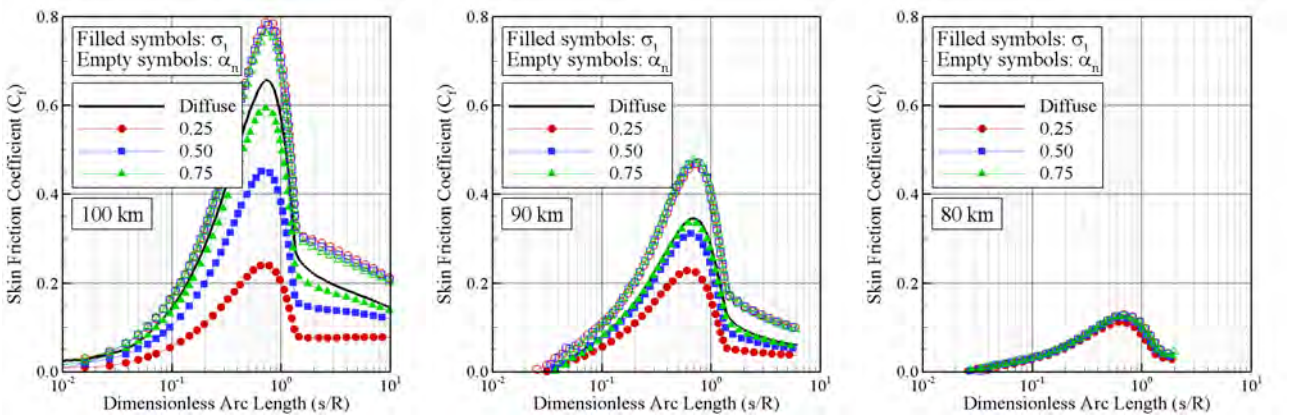

Figure 7. Skin friction coefficient (C_f) distribution along the capsule surface as a function of the surface accommodation coefficients for altitudes of (a) 100 km, (b) 90 km, and (c) 80 km.

ISSN 2176-5480

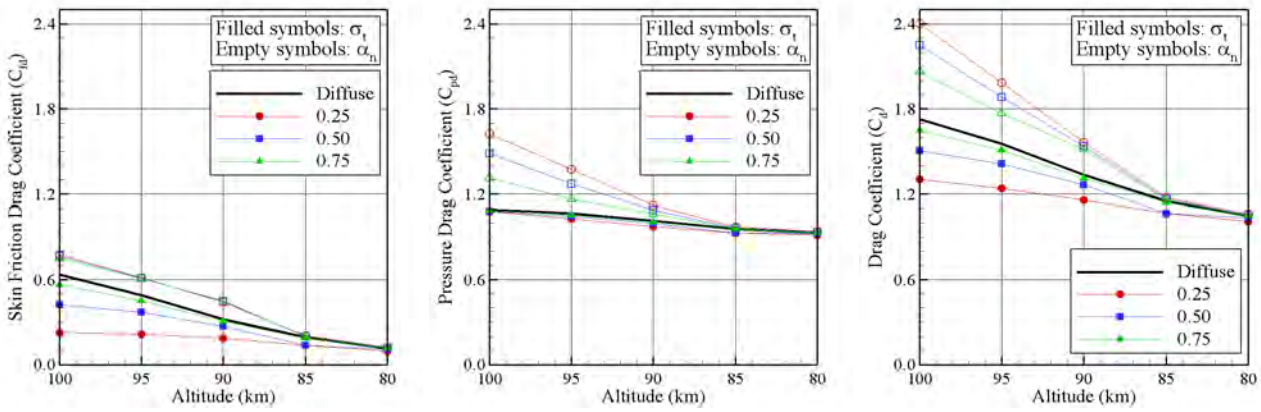

Figure 8. (a) Skin friction drag coefficient C_{fd}, (b) pressure drag coefficient C_{pd}, and (c) total drag coefficient C_d as a function of the altitude parameterized by the surface accommodation coefficients α_n and σ_t.

point, increases to a maximum value located on the spherical surface and decreases downstream along this surface up to the sphere/cone junction point. Larger altitude leads to higher peak value for the skin friction coefficient C_f. It is also seen that the skin friction coefficient C_f presents an opposite behavior from that of pressure coefficient in the sense that it decreases with reducing the tangential accommodation coefficient σ_t. Also of great significance is the skin friction changes on the conical afterbody surface with diminishing the tangential accommodation coefficient, in contrast to the pressure coefficient behavior. Furthermore, significant changes are observed in the skin friction coefficient C_f for a reduction on the normal accommodation coefficient from 1 to 0.25.

7.5 Drag Coefficient

The total drag coefficient C_d is defined as being,

$$C_d = \frac{F_D}{\frac{1}{2}\rho_\infty V_\infty^2 A} \tag{11}$$

where F_D is the resultant force acting on the capsule surface and A is a reference area.

The drag force F_D is obtained by the integration of the pressure p_w and shear stress τ_w distributions along the capsule surface. In the present account, the integration was considered from the stagnation point to the station that corresponds to the sphere/cone junction. As a result, the reference area A was considered as being the frontal area at this station. In addition, no base pressure effects were taken into account on the calculations.

Changes in the total drag coefficient C_d due to variations on the altitude, or on the Knudsen number Kn_R, are displayed in Fig. 8. In this set of diagrams, the contributions of the pressure C_{pd} and skin friction drag C_{fd} to the total drag coefficient C_d are also illustrated. According to these plots, it is noticed that, as the altitude decreases from 100 km to 80 km, the total drag coefficient C_d decreases, and the pressure drag coefficient C_{pd} plays a significant part in the total drag coefficient, a characteristic of a blunt body. It should be emphasized that the total drag coefficient C_d decreases as the altitude decreases because the denominator of Eq. (11) increases with an altitude reduction. On the other hand, the total drag force, F_D increases with a reduction in the altitude.

7.6 COMPUTATIONAL AND EXPERIMENTAL COMPARISONS

Having a clear qualitative picture of the aerodynamic surface properties, it proves instructive a comparison of these results with those available from experiments. However, this is not a simple task, given the small number of studies on SARA capsule. As a result, the alternative is a comparison of the simulation data with those obtained experimentally for a similar geometry, i.e., a body defined by a spherical nose with a conical afterbody. In view of this difficult, Figs. 9(a-b) display the pressure acting on the body surface for a similar geometry. In this set of figures, the wall pressure p_w is normalized by the pressure at the stagnation point p_o, and the arc length s along the body surface is normalized by the nose radius R. In addition, the pressure ratio corresponding to altitudes from 100 km to 80 km is related to the diffusion reflection case. Furthermore, Fig. 9(a) illustrates the pressure ratio p_w/p_o distribution with a linear scale in the abscissa, while Fig. 9(b) depicts the same pressure ratio distribution in a logarithm scale in order to emphasize the pressure ratio behavior at the vicinity of the stagnation point.

ISSN 2176-5480

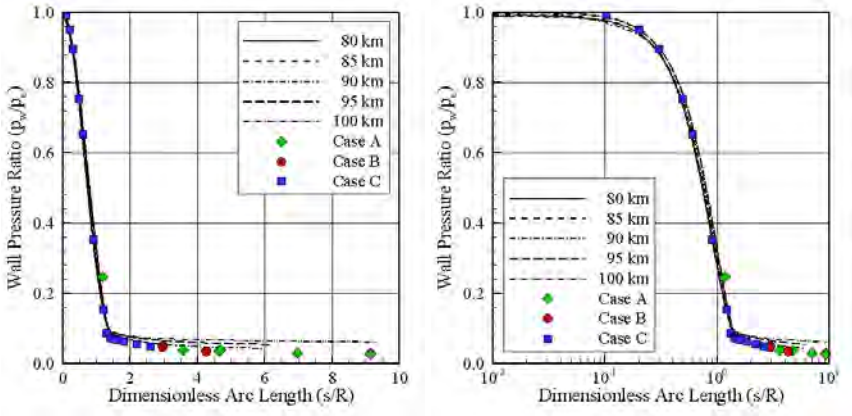

Figure 9. Comparison of wall pressure ratio (p_w/p_o) distribution along the body surface in a (a) linear scale and in a (b) logarithm scale.

Based on this set of figures, Case A (Griffith and Lewis, 1964) refers to experimental data obtained in the hypervelocity tunnel of the Arnold Engineering Development Center-von Kármán Facility (AEDC-VKF) for a 9-degree half-angle spherically blunted cone. In addition, N_2 was used as the working fluid, freestream Mach number near 19 and freestream Reynolds number between 8,000 and 15,000/in. Case B (Wilkinson and Harrington, 1962) corresponds to experimental data obtained from Cornell Aeronautical Laboratory (CAL) shock tunnel for a 9-degree half-angle spherically blunted cone, with air as a working fluid, freestream Mach number near 14.5 and freestream Reynolds number between 5,700 and 12,000/in. Finally, Case C (Machell, 1956) represents a spherical nosed cone with semi-vertex angle of 10 degrees tested in a hypersonic wind tunnel at a Mach number of 5.8, and freestream Reynolds number in the range of 0.97–2.38$\times 10^5$/in. Some characteristics of the models for Case A, B and C are tabulated in Table 3.

Table 3. Flow and geometric conditions for the spherically blunted cone models.

Case	A (Griffith and Lewis, 1964)	B (Wilkinson and Harrington, 1962)	C (Machell, 1956)
M_∞	~ 19	~ 14.5	5.8
Re_∞/in	$9 - 15 \times 10^3$	$5.7 - 12 \times 10^3$	1.910×10^5
R/R_B	0.3	0.3	0.8
θ	9	9	10

According to Figs. 9(a-b), it is clearly seen that the wall pressure ratio for the present work agreed reasonably well with that obtained experimentally. It is important to remark that the shape of the pressure distributions as described in nondimensional coordinates is independent of the spherical nose radius and of the Reynolds number over the range investigated.

8. CONCLUDING REMARKS

Computations of a rarefied hypersonic flow over the SARA capsule have been performed by using the Direct Simulation Monte Carlo method. The calculations provided information concerning the nature of the aerodynamic surface quantities by considering incomplete surface accommodation.

Effects of rarefaction on the number flux, heat transfer, pressure, skin friction and drag coefficients were investigated for an altitude range, covering a hypersonic flow from the free molecular flow regime to the transition flow regime. The altitude varied from 100 to 80 km, which correspond to Knudsen numbers Kn_R from 0.4615 to 0.0115, respectively. In addition, effects on the incomplete surface accommodation on the these surface properties were investigated for a representative range of normal and tangential accommodation coefficients. The normal and tangential accommodation coefficients varied from 1.0 to 0.25.

The analysis showed that the stagnation region is a thermally stressed zone, as expected. The peak value for the heat flux was attained at the stagnation point. It was also found that the stagnation region is a zone of strong compression, high wall pressure. In contrast, the peak value for the shear stress took place on the spherical nose surface, more precisely between the stagnation point and the sphere/cone junction.

ISSN 2176-5480

Calculations showed that a reduction in the normal accommodation coefficient from 1.0 to 0.25 decreased the heat transfer coefficient in the stagnation region. In contrast, a reduction in the tangential accommodation coefficient increased slightly the heat transfer coefficient in the stagnation region. Also, it was found that the total drag coefficient is reduced by a reduction in the tangential accommodation coefficient, and increased by a reduction in the normal accommodation coefficient for high altitudes.

9. ACKNOWLEDGMENTS

The author would like to thank the financial support provided by CNPq (Conselho Nacional de Desenvolvimento Científico e Tecnológico) under Grant No. 312094/2009-4.

10. REFERENCES

Alexander, F. J., Garcia, A. L., and Alder, B. J., 1998. "Cell Size Dependence of Transport Coefficient in Stochastic Particle Algorithms". Physics of Fluids, Vol. 10, No. 6, pp. 1540–1542.

Alexander, F. J., Garcia, A. L., and Alder, B. J., 2000. "Erratum: Cell Size Dependence of Transport Coefficient in Stochastic Particle Algorithms". Physics of Fluids, Vol. 12, No. 3, pp. 731–731.

Bird, G. A., 1981. "Monte Carlo Simulation in an Engineering Context". In Fisher, S. S., ed., Progress in Astronautics and Aeronautics: Rarefied gas Dynamics, Vol. 74, part I, AIAA New York, pp. 239–255.

Bird, G. A., 1989. "Perception of Numerical Method in Rarefied Gasdynamics". In Muntz, E. P., Weaver, D. P., and Capbell, D. H., eds., Rarefied Gas Dynamics: Theoretical and Computational Techniques, Vol. 118, Progress in Astronautics and Aeronautics, AIAA, New York, pp. 374–395.

Bird, G. A., 1994. Molecular Gas Dynamics and the Direct Simulation of Gas Flows, Oxford University Press.

Borgnakke, C. and Larsen, P. S., 1975. "Statistical Collision Model for Monte Carlo Simulation of Polyatomic Gas Mixture". Journal of Computational Physics, Vol. 18, No. 4, pp. 405–420.

Carlson, H. A., 1999. "Aerothermodynamic Analyses of Hypersonic Blunt-Body Flows". Journal of Spacecraft and Rockets, Vol. 36, No. 6, pp. 912–915.

Cercignani, C., 1972. "Scarrering Kernels for Gas-Surface Interactions". Transport Theory and Statistical Physics, Vol. 2, No. 1, pp. 27–53.

Cercignani, C. and Lampis, M., 1971. "Kinetic Models for Gas-Surface Interactions". Transport Theory and Statistical Physics, Vol. 1, No. 2, pp. 101–114.

Garcia, A. L., and Wagner, W., 2000. "Time Step Truncation Error in Direct Simulation Monte Carlo". Physics of Fluids, Vol. 12, No. 10, pp. 2621–2633.

Gilmore, M. R., and Crowther, R., 1995. "Direct Simulation and Test Particle Monte-Carlo, and Navier-Stokes Predictions of the Re-entry state of the FSW-1 Satellite". In Harvey, J. and Lord, G., eds., Proceedings of the 19th International Symposium on Rarefied Gas Dynamics, Oxford, University Press, Vol. 2, pp. 1387–1393.

Gnoffo, P., 1999. "Planetary-Entry Gas Dynamics". Annual Review of Fluid Mechanics, Vol. 31, pp. 459–494.

Griffith, B. J., and Lewis, C. H., 1964. "Laminar Heat Transfer to Spherically Blunted Cones at Hypersonic Conditions". AIAA Journal, Vol. 2, No. 3, pp. 438–444.

Gupta, R. N., Moss, J. N., and Price, J. M., 1996. "Assessment of Thermochemical Nonequilibrium and Slip Effects for Orbital Reentry Experiment (OREX)". In Proceedings of the 31st AIAA Thermophysics Conference, AIAA Paper 1996–1859, 17–20 Jun, New Orleans, LA.

Hadjiconstantinou, N. G., 2000. "Analysis of Discretization in the Direct Simulation Monte Carlo". Physics of Fluids, Vol. 12, No. 10, pp. 2634–2638.

Hedahl, M. O. and Wilmoth, R. G., 1995. "Comparison of the Maxwell and the CLL Gas-Surface Interacion Models using DSMC". NASA TM-110205.

Ivanov, M. S., Markelov, G. N., Gimelshein, S. F., Mishina, L. V., Krylov, A. N., and Grechko, N. V., 1998. "High-Altitude Capsule Aerodynamcis with Real Gas Effects". Journal of Spacecraft and Rockets, Vol. 35, No. 1, pp. 16–22.

Kozak, D. V., and Sharipov, F., 2012. "Aerothermodynamics of Satellite During Atmospheric Reentry for the Whole Range of Gas Rarefaction: Influence of Inelastic Intermolecular Collisions". Brazilian Journal of Physics, Vol. 42, pp. 192–206.

Longo, J. M. A., 2003. "Aerothermodynamics – A Critical Review at DLR". Aerospace Science and Techonology, Vol. 7, pp. 429–438.

Lord, R. G., 1991. "Application of the Cercignani-Lampis Scattering Kernel to Direct Simulation Monte Carlo Method". In Proceedings of the 17th International Symposium on Rarefied Gas Dynamics, edited by A. E. Beylich, pp. 1427-1433, 8 – 14 July, Aachen, Germany.

Machell, R. M., 1956. "An Experimental Investigation of Hypersonic Flow over Blunt Nosed Cones at a Mach Number of 5.8". In Aeronautical Engineer Thesis, CalTech, CA.

Maxwell, J. C., 1879. "On Stresses in Rarefied Gases Arising from Inequalities of Temperature". Philosophical Transac-

ISSN 2176-5480

tions of the Royal Society of London, Vol. 170, Pt. 1, pp. 231–256, reprinted in The Scientific Papers of J. C. Maxwell, Dover, New York, 1965.

Moss, J. N., Glass, C. E., and Greene, F. A., 2006. "Blunt Body aerodynamics for Hypersonic Low Density Flows". In Proceedings of the 25th International Symposium on Rarefied Gas Dynamics, Saint Petersburg, Russia.

Pimentel, C. A. R., Azevedo, J. L. F., Korzenowski, H., and Mantelli, M. B. H., 2005. "Chemical Equilibrium Inviscid Flow over SARA Re-Entry Vehicle". In Proceedings of the 43rd AIAA Aerospace Sciences Meeting and Exhibit, AIAA Paper 2005–0390, 10–13 Junuary, Reno, NV.

Santos, W. F. N., 2012. "Aerothermodynamic Analysis of a Reentry Brazilian Satellite". Brazilian Journal of Physics, Vol. 42, pp. 373–390.

Savino, R., Fumo, M. S., Paterna, D., and Serpico, M., 2005. "Aerothermodynamic Study of UHTC-Based Thermal Protection Systems". Aerospace Science and Techonology, Vol. 9, pp. 151–160.

Sharipov, F., 2003. "Hypersonic Flow of Rarefied Gas Near the Brazilian Satellite During its Reentry into Atmosphere". Brazilian Journal of Physics, Vol. 33, No. 2, pp. 398–405.

Tchuen, G., Burtschell, Y., and Zeitoun, D. E., 2005. "Numerical Prediction of Nonequilibrium Hypersonic Flow Around Brazilian Satellite SARA". Brazilian Journal of Physics, Vol. 35, No. 1, pp. 148–156.

Toro, P. G. P., Minucci, M. A. S., Ramos, A. G., Chanes Jr., J. B., Pereira, A. L., Korzenowski, H., Nagamatsu, H. T., and Myrabo, L. N., 2001. "Experimental Investigation of blunt Body at Mach 8". In Proceedings of the 39th AIAA Aerospace Sciences Meeting and Exhibit, AIAA Paper 2001–0644, 8–11 Junuary, Reno, NV.

Toro, P. G. P., Minucci, M. A. S., Chanes Jr., J. B., and Ramos, A. G., 2004. "Experimental Hypersonic Investigation over the Micro-Satellite SARA". In Proceedings of the 10th Brazilian Congress of Thermal Sciences and Engineering, Rio de Janeiro, RJ, Brazil.

Vashchenkov, P. V., and Ivanov, M. S., 2002. "Numerical Analysis of High-Altitude Aerothermodynamics of Expert Reentry Vehicle". In Proceedings of the International Conference on the Methods of Aerophysical Research, Russia.

Weiland, C., Longo, J., Gülhan, A., and Decker, K., 2004. "Aerothermodynamics for Reusable Lanch Systems". Aerospace Science and Techonology, Vol. 8, pp. 101–110.

Wilkinson, D. B. and Harrington, S. A., 1962. "Hypersonic Force, Pressure and Heat Transfer Investigations of Sharp and Blant Slender Cones". Rept. AF-1560-A-5, Cornell Aeronaut. Lab.

Wilmoth, R. G., Mitcheltree, R. A., and Moss, J. N., 1997. "Low-Density Aerodynamics of the Stardust Sample Return Capsule". In Proceedings of the 32nd AIAA Thermophysics Conference, AIAA Paper 1997–2510, 23–25 Jun, Atlanta, GA.

Wood, W. A., Gnoffo, P. A., and Rault, D. F. G., 1996. "Aerodynamic Analysis of Commercial Experiment Transporter Re-Entry Capsule". Journal of Spacecraft and Rockets, Vol. 33, No. 5, pp. 643–646.

Woronowicz, M. S. and Rault, D. F. G., 1994. "Cercignani-Lampis-Lord Gas-Surface Interacion Model: Comparisons between Theory and Simulation". Journal of Spacecraft and Rockets, Vol. 31, No. 3, pp. 532–534.

11. RESPONSIBILITY NOTICE

The author is the only responsible for the printed material included in this paper.